Lab on a Chip

PAPER

View Article Online
View Journal | View Issue

Cite this: *Lab Chip*, 2019, **19**, 2512

Automated "pick and transfer" of targeted cells using dielectrophoresis

Rucha Natu,[a] Monsur Islam,[ab] Devin Keck[a] and Rodrigo Martinez-Duarte *[a]

Received 29th April 2019,
Accepted 24th June 2019

DOI: 10.1039/c9lc00409b

rsc.li/loc

Selective manipulation of single cells is an important step in sample preparation for biological analysis. A highly specific and automated device is desired for such an operation. An ideal device would be able to selectively pick several single cells in parallel from a heterogeneous population and transfer those to designated sites for further analysis without human intervention. The robotic manipulator developed here provides the basis for development of such a device. The device in this work is designed to selectively pick cells based on their inherent properties using dielectrophoresis (DEP) and automatically transfer and release those at a transfer site. Here we provide proof of concept of such a device and study the effect of different parameters on its operation. Successful experiments were conducted to separate *Candida* cells from a mixture with 10 μm latex particles and a viability assay was performed for separation of viable rat adipose stem cells (RASCs) from non-viable ones. The robotic DEP device was further used to pick and transfer single RASCs. This work also discusses the advantages and disadvantages of our current setup and illustrates the future steps required to improve the performance of this robotic DEP technology.

1. Introduction

The selective isolation and spatiotemporal manipulation of targeted cells is important towards extracting complex information about how the cells interact and perform specialized functions. The spatiotemporal control of cells has especially gained importance due to the emphasis on studying cell heterogeneity, since phenotype heterogeneity between genetically identical cells is known to play an important role in tumour metastasis, drug resistance, clinical diagnosis, cell differentiation and cell functionality.[1,2] Hence, a few manipulation techniques have been developed in recent years to gain spatiotemporal control of cells in a suspension. Optical tweezers are widely used,[3,4] but they are limited in their capability to identify targeted cells due to the minor differences between the refractive index of cells and that of their suspending medium. Furthermore, the hardware can be complex, especially when implementing several parallel traps. Micromanipulation techniques such as microrobotic arms, microgrippers and mobile microrobots exhibit precise control in transporting micro/nano particles, but they are also limited in terms of parallelization and cell identification.[5–9] Indeed, the image analysis used in these techniques is limited to identifying cells based on size and morphology, or by using stains specific to the targeted cell. Liquid handling robots, or robotic pipettes, enable the precise, automatic and reproducible transfer of minute amounts of liquids that may contain cells, but sorting is again restricted to image analysis. Therefore, there is still a need for high specificity when attempting to gain spatiotemporal control of targeted cells.

Dielectrophoresis (DEP) is a label-free technique used for cell sorting in a wide range of applications.[10,11] When cells are exposed to an electric field gradient of a given frequency they respond by moving towards the strongest gradient, as in positiveDEP, or away from it as in negativeDEP.[11] Since the strength and direction of this response largely depend on the cell membrane capacitance, DEP can provide a high degree of specificity when discriminating targeted cells from their background. Indeed, the cell membrane capacitance has been shown to vary even when differences in size and appearance of cells are not discernible. One particularly useful and straightforward embodiment of DEP is a viability assay without the need for stains.[12–17] Other selected examples include the studies by Flanagan *et al.*[18,19] who showed changes in capacitance according to cell age and generation even when cell size remained the same; by Thomas *et al.* who isolated human osteoblast-like cells from a heterogeneous cell population using DEP-based cages;[20] by Srivastava *et al.* who studied the DEP response of red blood cells to identify blood types;[21] by Pethig *et al.* who used DEP for distinguishing cells with up to 3 mF m^{-2} difference in membrane capacitance;[22] and by Labeed *et al.*[23] who distinguished between cells with capacitance differences of around 2.3 mF m^{-2}. The successful

[a] *Multiscale Manufacturing Laboratory, Department of Mechanical Engineering, Clemson University, SC 29634, USA. E-mail: rodrigm@clemson.edu*
[b] *Karlsruhe Institute of Technology, Institute of Microstructure Technology, Hermann-von-Helmholtz-Platz 1 76344, Eggenstein-Leopoldshafen, Germany*

usage of DEP for enrichment of targeted cells from heterogeneous populations[20] and rare cell isolation[24] further highlights the high specificity achievable of this technique. In terms of DEP technology, most of the work on DEP-based separations has been done in traditional flow-through microfluidic systems.[25] In particular, Manaresi *et al.* reported a single cell manipulation microfluidic platform using a CMOS chip to capture individual cells in DEP-enabled cages,[26] which is currently commercialized as DEPArray™ by Silicon Biosystems. On the other hand, a few authors have implemented DEP-enabled tweezers by mounting wire electrodes on micromanipulators,[27–29] but such systems featured a single DEP trap or were largely manual, thus limiting their applicability.

In this work, the authors report the use of DEP traps mounted on a robotic manipulator, referred to as roboticDEP here, to automate the selective pick and transfer of cell populations and single cells between two different and separate liquid samples. An array of carbon microelectrodes was mounted on an XYZ robot to function in a manner similar to that of liquid handling robots: the array is immersed in a cell suspension to pick targeted cells, retracted from the suspension, moved a specific distance, and immersed in a separate liquid medium to place and transfer cells. RoboticDEP affords spatiotemporal control of targeted cells and significantly differs from traditional flow-through DEP devices where electrode arrays are contained within a microfluidic network. The use of pick and transfer principles instead of traditional microfluidics is expected to eliminate practical problems in microfluidic devices and enable better chances of integration with existent laboratory infrastructure used in sample preparation. For example, the use of liquid handling robots (LHRs) is prevalent in biological laboratories to transfer cells and liquids between different test stations, and the

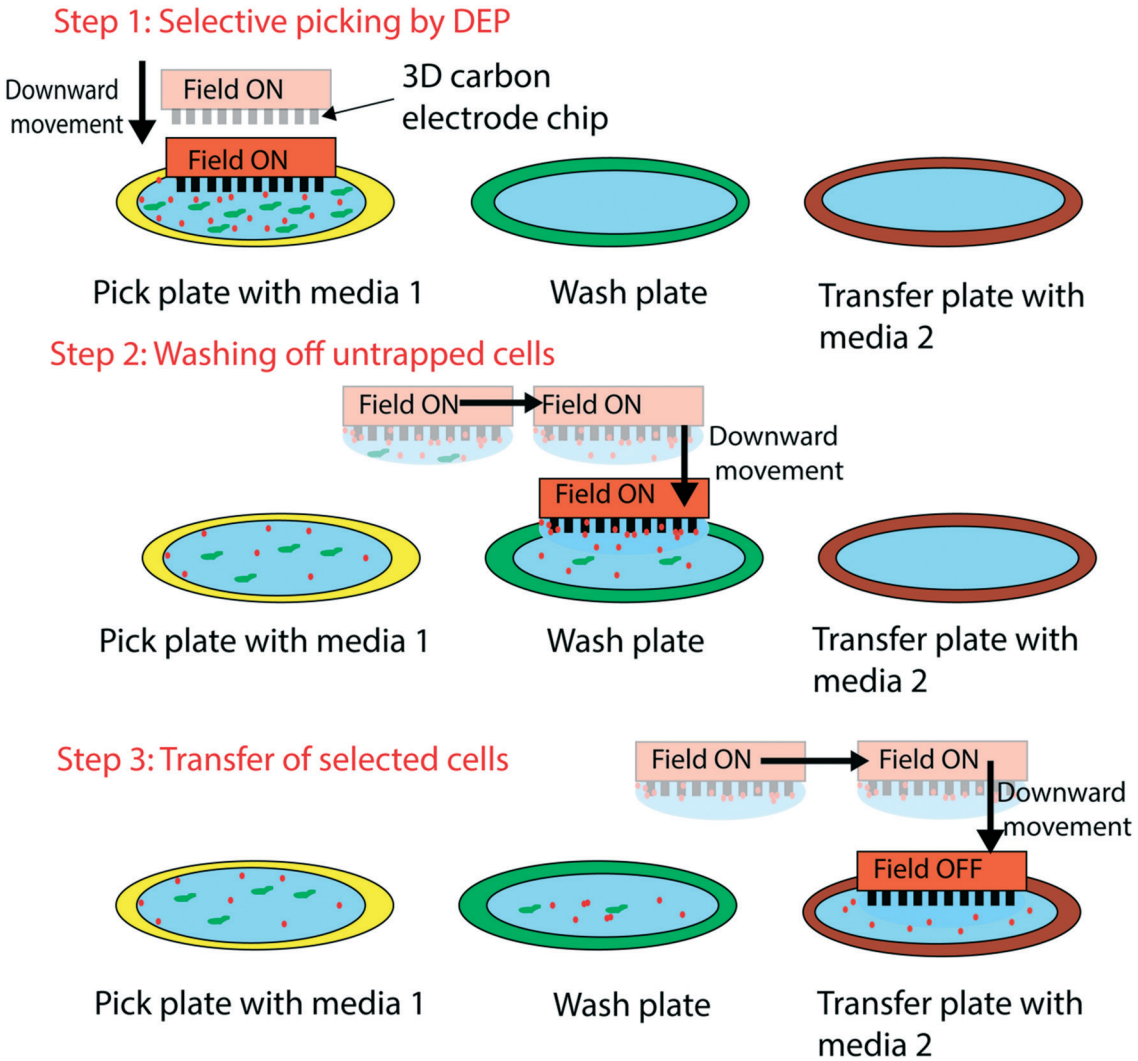

Fig. 1 Schematic of the roboticDEP device with the three steps: pick, wash and transfer. In the first step, the cells of interest (shown by red circles) are picked by the cylindrical electrodes using DEP force. In the second step, the picked cells are swept through the wash plate to wash off the non-specifically adhered cells (shown in green). In the third step, the cells transferred to the transfer plate are released by switching off the DEP field.

concept of roboticDEP can develop into a complement to LHRs to automatically and selectively pick and transfer the cells of interest to desired sites. Here, we demonstrate the proof of concept of roboticDEP and delve into the parameters that affect the performance of each of its steps. Experiments at the population level were conducted to (a) pick and transfer infectious yeast cells *Candida albicans* and *Candida tropicalis*; (b) separate *C. tropicalis* from a mixture with polystyrene particles; and (c) separate viable and non-viable rat adipose stem cells (RASCs) based on the difference in their DEP properties. We further demonstrate automated pick and transfer of viable single rat adipose stem cells from a population, an important step towards the use of roboticDEP for single-cell sample preparation.

2. Technology concept and supporting theory

The working principle for roboticDEP is a three-step process as illustrated in Fig. 1. In the first step, or pick step, the targeted cells are picked up from a suspension in medium 1 by attracting them to the electrodes using DEP. Here we demonstrate roboticDEP using 3D cylindrical carbon electrodes (~100 μm in height) but no restriction on the type of material for future systems is envisioned. In the second, or wash step, the electrode array is swept through a wash solution to remove those cells non-specifically adhered to the electrodes. In the third step, or transfer, the array is immersed in medium 2 and cells attached to the electrodes by DEP are released onto the wash plate by switching off the electric field. Throughout the process, the cells are exposed to a DEP force due to polarization of the array and a drag force due to the movement of the array through the liquid medium. The interaction between these forces must be understood and controlled to enable pick and transfer. Also important is the control of the electric field and shear stress acting on the cells to prevent their inactivation.

The DEP force F_{DEP} for a cell approximated as a spherical particle (eqn (1)) depends on the radius of the cell r_p, the gradient of the square of the electric field ∇E_{rms}^2, and the permittivity of the medium ε with Re[f_{CM}] the magnitude of the real part of the Clausius–Mossotti factor [f_{CM}] given by eqn (2). The squared electric field gradient E_{rms}^2 is dependent on the electrode geometry and is proportional to the magnitude of the polarizing voltage and the gap between electrodes.[30] The value of [f_{CM}] depends on the particle and medium properties. Here, ε_p^* > and ε_m^* denote the complex permittivity of the cell and medium, respectively, σ denotes the conductivity, i represents the imaginary number $\sqrt{-1}$ and the polarizing frequency is represented by f. The value of Re[f_{CM}] is the DEP cell signature that depends on the membrane capacitance and the frequency of the polarizing field. Depending on the sign of Re[f_{CM}], the DEP force can be either positive, in which the cells are attracted to the field gradient, or negative, in which they are repelled from it. Since the field gradient is usually strongest around the electrodes, positiveDEP usually denotes movement towards the electrodes, while negativeDEP denotes otherwise.

$$F_{DEP} = 2\pi r_p^3 \varepsilon \mathrm{Re}[f_{CM}] \nabla E_{rms}^2 \quad (1)$$

$$f_{CM} = \frac{\varepsilon_p^* - \varepsilon_m^*}{\varepsilon_p^* + 2\varepsilon_m^*} \quad \text{where } \varepsilon^* = \varepsilon + \frac{i\sigma}{2\pi f} \quad (2)$$

Besides DEP force, the cells will also be under the influence of a Stokes drag force expressed in eqn (3) where v is the velocity of the fluid around the electrodes during the wash step, μ is the dynamic viscosity of the medium and u_p is the particle velocity.

$$F_{DRAG} = 6\pi\mu r_p (v - u_p) \quad (3)$$

For the particles trapped on the electrodes, the particle velocity $u_p = 0$. During transfer, it is crucial that the cells that are trapped by DEP remain secured to the electrode, while the cells non-specifically captured are washed off. Thus, the drag force acting on the targeted cells should be smaller than the DEP force. The maximum value of v at which the cells captured by DEP remain captured at the electrodes during the wash is obtained by equating the drag force (eqn (3)) acting on the particle with the DEP force (eqn (1)). Thus, the maximum value of v_{max}, under which a targeted cell remains trapped on the electrode is expressed as

$$v_{max} \leq \frac{2\pi\varepsilon \mathrm{Re}[f_{cm}] r_p^3 \nabla E^2}{6\pi r_p \mu} \quad (4)$$

Along with the speed of the cell manipulation, the electric field and the amount of electric field exposure to the cell are of importance.[31] The electric field must be monitored to ensure cell viability, as prolonged exposure to the electric field can render the cells non-viable. When the cell is exposed to the external electric field, a transmembrane potential is induced in the cell. If this potential is greater than a threshold value, dependent on cell type and likely >1 V, the cell membrane can be compromised.[32] For example, in DEP experiments conducted on neural stem cells, Lu *et al.* reported that cell exposure at 8 V peak to peak at frequencies of 50–100 kHz (with electric field ~10^5 V m^{-1}) for time >5 min can affect the cell viability.[19] Hence, it is necessary to control the magnitude of the electric field loading the cell throughout the experimental device to guarantee cell viability. As a reference, the critical electric field strength that is required for a transmembrane potential of 1 V is 1 kV cm^{-1}.[33]

The shear stress acting on the cells can also affect their viability during the process. In the presented roboticDEP platform, the cells encounter maximum shear stress during the wash step in the region between the electrodes. Since the

flow in the region between the electrodes during the wash step is expected to resemble Poiseuille's flow with electrode walls acting as the flow boundaries, the shear stress τ can be calculated using eqn (5):

$$\tau = \mu \frac{dv}{dx} \quad (5)$$

where the x-axis is taken perpendicular to the direction of the flow. Shear stress on the cell must be maintained below a threshold throughout cell manipulation. For example, the physiological levels of shear stress in the aortas of adults and embryos have been observed as 15 and 5 dyne per cm^2, respectively, though magnitudes down to 1.5 dyne per cm^2 are known to affect adult blood phenotypes.[34–36] An exposure to shear stress of 1.5 to 15 dyne per cm^2 for over two days was also reported to result in differentiation of embryonic stem cells.[37]

3. Materials and methods

3.1 Experimental setup

The array of 3D carbon microelectrodes was fabricated *via* carbonizing the SU-8 microstructures previously made using photolithography. The use of these carbon electrodes in dielectrophoresis is well established and details on their fabrication and performance are reported elsewhere.[13,15,38–48] Briefly, microstructures were fabricated by a two-step photolithography process of SU-8 (Gersteltec, Switzerland), a negative-tone photoresist, on a silicon wafer substrate. These structures were then carbonized by heat treatment to 900 °C in a nitrogen atmosphere. The rectangular shaped electrode array featuring a footprint of around 6 mm by 1 mm with 100 rows and 10 columns featured an intercalated organization of electrodes, each of which is 100 μm in height and 50 μm in diameter separated by 115 μm centre-to-centre distance. Planar carbon leads were fabricated to connect the base of all 3D electrodes to large carbon pads to facilitate the connection of the array to the signal generator (see Fig. 2B). Electrodes were polarized alternately as shown in Fig. 2F. The carbon pads were then manually coated with a thin layer of indium and covered with copper tape (~70 μm thick). The indium was used for the connection between the carbon pads and the copper tape. The copper tape was then coated with epoxy to prevent contact with the experimental samples. The copper tape was further connected to the signal generator (BK Precision 4054, BK Precision, CA, USA) through an adaptor mounted on the header (see device schematic in Fig. 2B). The silicon substrate containing the array and connections was then mounted on a header made out of high impact polystyrene (HIPS) using fused deposition modelling (Lulzbot Taz 5).

The experimental roboticDEP platform used in this work is illustrated in Fig. 2A. The base of the system was an A2 Delta 3D printer (Afinibot, Shenzhen, China) featuring a step size of 100 μm and a speed of movement between 1 and 100

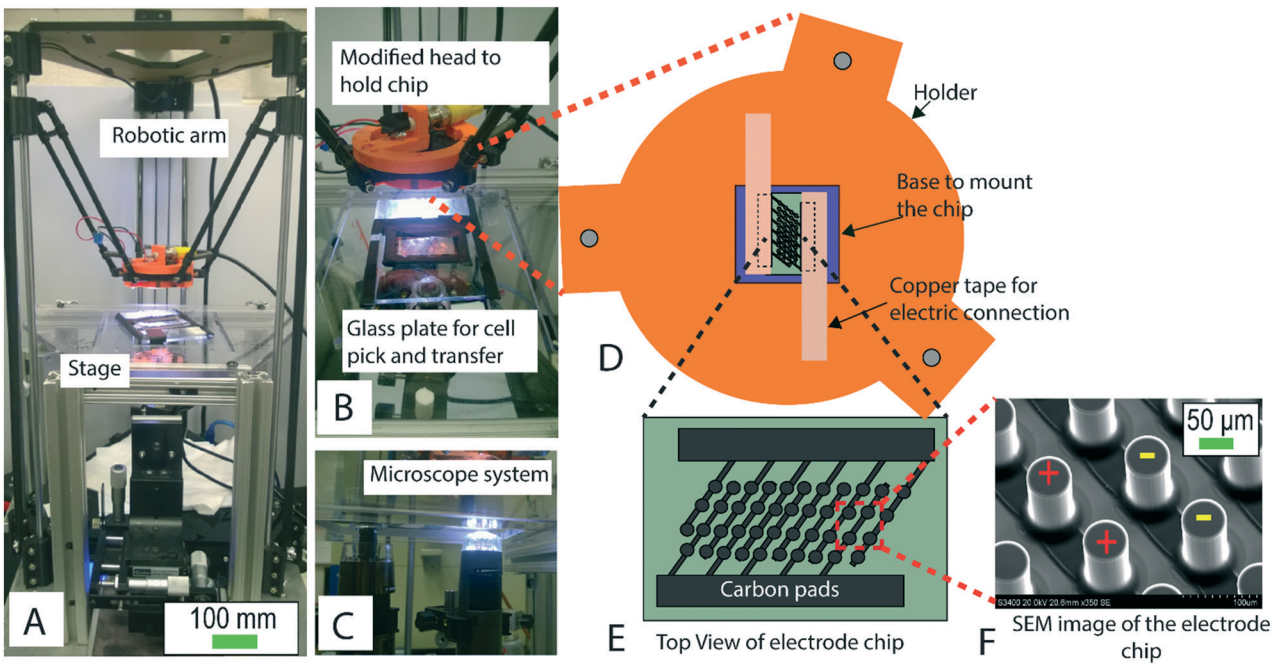

Fig. 2 (A) The 3D printer used here as a robotic manipulator emphasizing the robotic arm and the stage. The stage hosts the glass plate for the experiment. (B) The modified printer head that holds the 3D carbon electrode array. The glass plate on the stage is divided into three sections, pick, wash, and transfer, separated by black electrical tape. (C) Two microscopes are positioned below the stage for imaging: one below the pick section and another below the transfer section. (D) The modified printer head hosts the electrode chip and the electrical connections. (E) Schematic showing the top view of the carbon electrode chip and the SEM image showing the electrode structure and the connecting lines. (F) Scanning electron microscope image of the carbon electrode array showing the polarization scheme used for the experiments.

mm min^{-1}. The original printing head was replaced by the header containing the electrode array (see Fig. 2). The footprint of the electrode area on the chip was approximately 6.5 mm^2, and the footprint of the header was approximately 1600 mm^2. The path trajectory taken by the header was programmed using the Repetier host software that is part of the 3D printer package. The stage consisted of a glass plate divided into three sections, for pick, wash and transfer. A microscope (AM7515MT8A, a 5MP Dino-Lite Edge Series Microscope, CA, USA) was mounted below each of the pick and transfer sections to monitor the experiment and capture the images of the cells being selected and released.

3.2 Preparation of experimental samples

Different particle suspensions were used as experimental samples in this work: (1) *Candida albicans*, (2) *Candida tropicalis*, (3) a mixture of *C. tropicalis* and 10 μm diameter latex particles, and (4) a mixture of viable and non-viable rat adipose stem cells (RASCs). *C. albicans* and *C. tropicalis* were independently cultured in yeast malt broth (YMB) (Sigma Aldrich Y3752) with 5% glucose. Cells were passaged every three days to keep the cell culture thriving. After passage, cells were used after 24 hours for the experiments. Cells were washed with DEP medium solution using centrifugation. The stock DEP medium solution was prepared with 200 ml distilled water by adding 18 g sucrose, 0.5 g dextrose and 0.3 g bovine serum albumin (BSA).

The measured average cell size (diameter) for *C. albicans* and *C. tropicalis* was 5.12 ± 0.75 μm and 5.98 ± 0.75 μm, respectively, which was in accordance with previous reports.[49] The experimental *Candida* samples for DEP were prepared by resuspending the cultured cells in a sugar solution using three cycles of solution exchange aided by centrifugation. The *Candida* experimental samples featured an electrical conductivity of 2×10^{-3} S m^{-1} and a cell concentration of $\sim 10^5$ cells per ml. Preliminary experiments using a traditional microfluidics-based DEP system showed a positiveDEP response of *C. albicans* at frequencies of 50–1000 kHz with a peak at 100 kHz. Similarly, *C. tropicalis* showed positiveDEP at f = 50–1000 kHz, peaking at 200 kHz.[50] The 10 μm diameter latex particles used in the mixture with *C. tropicalis* were obtained from Magsphere (catalog #PS010UM). It is widely known that such particles experience negativeDEP throughout the frequency spectrum from a few kHz to tens of MHz.[51–53] This experimental sample featured a concentration of $\sim 10^5$ particles per ml, with 15% particles and 85% *C. tropicalis*, and an electrical conductivity of 2×10^{-3} S m^{-1}.

Rat adipose stem cells (RASCs) were obtained from the Cell and Tissue Culture Laboratory in the Bioengineering Department at Clemson University. The cell strains were cultured in Dulbecco's Modification of Eagle's Medium (DMEM) ×1, 1% antibiotic antimycotic solution (Mediatech, Inc., Manassas, VA), and 10% culture supplement (Discovery Labware Inc, Bedford, MA) for 5 days to obtain a confluent cell culture in 5 ml flasks. Non-viable cells were obtained by heat treatment at 70 °C for 20 min. The experimental sample was obtained by resuspending viable and non-viable cells in the stock DEP medium and adjusting the electrical conductivity to 1.2×10^{-2} S m^{-1} using PBS solution prepared by dissolving 1 tablet of phosphate-buffered saline (PBS) (Sigma Aldrich P4417) in 200 ml of distilled water. The viability of RASCs was determined with a Live/Dead Viability/Cytotoxicity Kit (Thermo Fisher Scientific, Waltham, MA) prepared with 20 μl of 2 mM EthD-1 and 5 μl 4 mM calcein AM in 10 ml sterile tissue culture-grade D-phosphate-buffered saline (PBS) (Thermo Fisher Scientific, Waltham, MA). The average size (diameter) of viable RASCs was 20 μm ± 2 μm, while that of non-viable RASCs was 20 μm ± 4 μm. The experimental sample featured an average of 30/70 percentage ratio of viable to non-viable cells. Preliminary experiments (data not shown) at the conductivity of 1.2×10^{-2} S m^{-1} showed viable RASCs exhibiting a positive DEP while the non-viable ones showed a negative DEP at frequencies of around 100 kHz. The details of all the experimental samples used here are summarized in Table 1.

3.3 Experimental protocol

The experiment was set up as follows to feature three different stages: (1) pick, (2) wash and (3) transfer, which were implemented using compartments made of acrylic plastic. The pick section consisted of a glass surface where ~10 μl of cell suspension at a concentration of ~400 cells per mm^2 were initially deposited by manual pipetting. The wash section was also a glass surface featuring 5 ml of cell-less DEP medium. The transfer section featured a haemocytometer (Hausser Scientific with Neubauer scale), used as a measurement grid, on which ~10 μl of cell-less DEP medium were deposited by manual pipetting. Cell counting was directly performed on the haemocytometer (after placing the cover glass) once the transfer step was finished.

The robotic arm was programmed to move through the three sections in sequence. The robotic arm first moved the electrode array over to the pick section and lowered the array to introduce it into the drop of cell suspension. The electric field was then switched on to selectively trap the cells of interest using DEP, allowing for 1 min at a stationary condition to complete any trapping. The robotic arm then retracted the electrode array from the pick section, moved it over to the wash section, and lowered the array with trapped cells into the cell-less DEP medium. Here, the arm was programmed to perform a back and forth motion at a designed speed to enable the non-specifically adhered cells on the chip to be washed off. The maximum speed used here was calculated using eqn (4) to curb shear stress on the cells and would ultimately depend on the type of cells used (see details in section 3.5). One back and forth motion of the robotic arm constituted one wash run. The number of runs was varied to study the effect of the wash time on the performance of the wash step. In the third and final step, the robotic arm retracted the electrode array from the wash

Table 1 Details of the samples used for different experiments

Cell composition	Medium conductivity in S m^{-1}	Approximate cell concentration
C. albicans or C. tropicalis	2×10^{-3}	10^5 cells per ml
C. tropicalis and 10 μm latex particles	2×10^{-3}	10^5 particles per ml; 85% particles and 15% cells
Viable and non-viable RASCs	1.2×10^{-2}	10^5 cells per ml; 70% non-viable and 30% viable cells
Viable RASCs	2×10^{-3}	10^3 cells per ml

solution, moved over to the transfer section, and introduced the array into the cell-less DEP medium on the transfer plate. The electric field was then switched off to release the cells and place them on the transfer plate. One minute at stationary condition was provided to allow for the cells to be released from the electrodes and dispersed in the medium. Alternatively, the electrodes were polarized with a different frequency to induce a negativeDEP behaviour on the cells and thus actively repel them from the electrodes for placing. The entire process just described took about 4 minutes and the cells remained exposed to the electric field for less than 3 minutes. Of note, the speed of the robotic arm was adjusted to 100 mm min^{-1} for movements between the different sections. However, it was reduced to 1 mm min^{-1} as it approached the pick, wash or transfer sections to reduce the possibility of impact with the glass or with the medium.

3.4 Data analysis

The number of cells on each of the 1 mm^2 corners of the Neubauer grid on the haemocytometer was counted for data analysis. At least three experiments were performed for each data point and the average value for the experiments is reported here. In the case of the experiments with separation of cells and particles, the percentage of each species was calculated using eqn (6);

$$\%\ \text{of cells in transfer section} = \frac{\text{Total count of cells at transfer section}}{\text{Total count of cells + total count of particles at the transfer section}} \quad (6)$$

The images provided in the Results section were obtained after processing the images captured with the microscopes. Specifically, we increased the image brightness using DinoCapture software (as provided with the Dino-Lite microscopes used here) since the amount of light reflected by the cells in the experiment was low. The images captured when manipulating RASCs were transformed to a negative image and the contrast and sharpness of the image were adjusted for better visibility.

3.5 Computational model

COMSOL Multiphysics 4.4 (Stockholm, Sweden) was used to independently model both the flow and the electric field in an array of electrodes with dimensions equal to those of the experimental device used here. Hence, the diameter of the electrode was 50 μm, and the centre-to-centre spacing between the electrodes was 115 μm. While the experimental array featured 100 × 10 electrodes, we simplified the model to 20 × 10 electrodes, which represents 1/5th of the original chip length. The variation in flow mainly occurs in the region between the electrodes, in the direction of the movement of the chip. The flow profile in the direction along the height of the electrode is not expected to show a major variation. Since the influence of electrode cross section surpasses the effect of electrode height in this case, a 2D model with cross sections of the electrodes is used to represent the domain of interest. An Intel® Xeon® CPU E5-1650 v2 @ 3.50GHz processor with a RAM of 32 GB and a 64 bit operating system was used for these simulations. A mesh with a maximum element size of 30 μm was selected after performing a grid independence study (data not shown). In the operation of the actual device, the electrode array attached to the robotic arm through the header moves back and forth in the medium in the wash plate, with a given speed U. However, in the simulation the chip was assumed stationary and the fluid flowing at velocity U. The laminar flow module was used to compute the velocity in the domain given by v and the average velocity v_{avg} in the region between electrodes. v will vary at different points in the domain, based on the velocity U, electrode geometry and distance of the point of interest from the electrodes. The average velocity v_{avg} in the domain is calculated my taking a mathematical average of values of v across the domain. Thus, v_{avg} also depends on U. The model used the Navier–Stokes equation and the continuity equation at steady state, given by eqn (7) and (8), where the fluid density is denoted by ρ and p is the pressure.

$$\rho(v\cdot\nabla)v = -\nabla p + \mu\nabla^2 v \quad (7)$$

$$\rho\nabla\cdot v = 0 \quad (8)$$

Eqn (7) and (8) were solved in COMSOL to obtain the velocity U in the domain. The average velocity v_{avg} obtained from COMSOL simulation was compared with the value of v_{max} (eqn (4)). If $v_{avg} \leq v_{max}$ the captured cells will remain captured and the uncaptured cells will be washed away. The speed of the robotic arm U and v_{avg} can be correlated to understand the relation between the speed of the robotic arm and the velocity obtained around the electrodes. Eqn (5) was used to compute the shear stress in the domain in the region close to the electrodes where the cells are expected to be captured.

The electric field in the domain was computed using the electric currents module with a stationary study in COMSOL

as detailed in our previous work.[54] The significance of computing the electric field in this domain was only to ensure that the electric field does not exceed 1 kV cm^{-1} near the electrodes; which is the limit of field strength at which the cell membrane can be compromised.

4. Results

4.1 The occurrence of non-specific cell transfer despite the selection and transfer of cells

The first objective was to validate the transfer of different *Candida* strains when using a DEP force to selectively pick them from suspension, wash them and transfer them. Results are shown in Fig. 3 when using one wash cycle and a header speed of 0. 0017 m s^{-1} through the washing. We first assessed the effect of the polarizing voltage on the transfer of *C. albicans* (Fig. 3A) at a given frequency of 100 kHz; second, we characterized the transfer throughput depending on the signal frequency (Fig. 3B) at a given voltage of 20 Vpp; and third, we evaluated the transfer of *C. tropicalis* depending on the signal frequency (Fig. 3C) and also at a voltage of 20 Vpp. Of note, the voltage drop across carbon electrodes used here was influenced by the resistivity of the carbon used here (~1 × 10^{-4} Ω m (ref. 55)). Based on previous analysis of this particular electrode design,[47] we considered a voltage drop of 25% at the surface of the microelectrodes compared to that delivered by the function generator. The voltage values reported in this work are the peak-to-peak values of the sinusoidal signal delivered by the function generator. The root mean square (RMS) value of the voltage in the domain

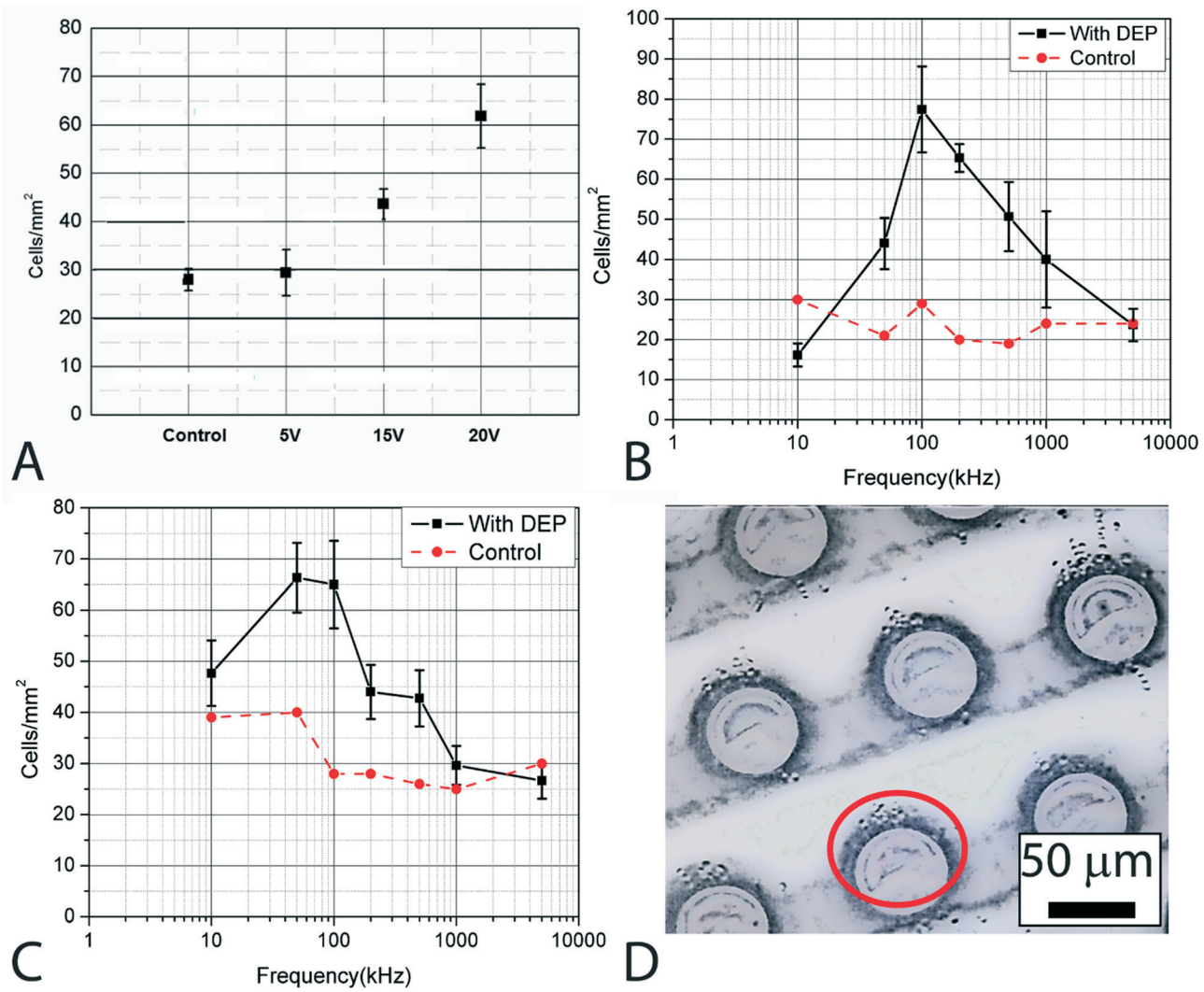

Fig. 3 (A) The output as obtained at different voltages in the experiment with an expected increase in *C. albicans* cell output with an increase in the applied voltage. (B) The capture and transfer behaviour for the *C. albicans* cells with the DEP frequency change. The control indicates the number of cells transferred without DEP changes (*i.e.* from the liquid wetting of the device) and the number of cells transferred to the placement section with DEP changes with an increase in frequency with the maximum transfer occurring at 100 kHz. (C) The behaviour of capture and transfer for the *C. tropicalis* cells with the change in DEP frequency, in which the control indicates the number of cells transferred without DEP. (D) *C. albicans* captured at the electrodes during the pick step.

corresponding to the sinusoidal signal was 10.6 V and the corresponding maximum electric field was around 0.9 kV cm^{-1}. Analysis of Fig. 3A shows how the transfer throughput in cells per unit area was directly proportional to the voltage used to polarize the electrode array. This was expected since using a higher voltage at a given frequency yields a stronger DEP force. Using a voltage down to 5 Vpp did not lead to significant DEP trapping. The results from the control experiment also suggest that cells could be transferred due to non-specific adhesion. In terms of the impact of frequency, results for both *Candida* strains clarify how the transfer throughput depends on the properties of the cell. The DEP force was its strongest at 100 kHz for *C. albicans* and at 50 kHz for *C. tropicalis*. As the frequency increased or decreased away from these peaks, the DEP force for both *Candida* strains decreased. We observed *C. albicans* and *C. tropicalis* cells moving away from the electrodes below 10 kHz and no effective movement was observed above 5 MHz, resulting in the negative differences between experiments and control in Fig. 3B and C. Hence, cell transfer is possible with roboticDEP and both voltage and field frequency affect the transfer throughput attainable. However, the control experiments in Fig. 3A–C clearly indicate cell transfer in the absence of DEP. Similar levels of transfer were observed regardless of cell strain. It is possible that such behaviour occurred due to non-specific adhesion of the cells to the electrodes and/or other surfaces of the device such as the copper tape. Another possibility was non-specific cell adhesion to the device. Thus, we proceeded to investigate the conditions under which a wash of the electrode array after cell picking will be most efficient to minimize non-specific transfer.

4.2 The washing step must be optimized to remove the non-specific transfer cells

As the electrode array mounted on the header travelled through the buffer on the wash plate, the cells were subjected to a drag force from the displaced fluid. Hence, one must be careful with how strong the wash is in order not to lose the cells picked in the previous step using DEP. Ideally, the drag force will only wash away those cells non-specifically adhered to the electrode array and device surface. Using eqn (7) and (8) and replicating our previous results,[44] we calculated and plotted the average fluid velocity in the region between the electrodes in the chip for different header speed U in the range 100–5000 mm min^{-1} (0.0017–0.083 m s^{-1}). Results are shown in Fig. 4A. The horizontal dashed lines represent the maximum fluid velocity permissible for different gradients of electric fields, as calculated using eqn (4) using r_p = 2.5 μm and $\mathrm{Re}[f_{CM}]$ = 0.75. This value of $\mathrm{Re}[f_{CM}]$ was approximated from the response of *S. cerevisiae* yeast cells at an f = 100 kHz since the dielectric parameters that would allow for modelling the DEP behaviour for *C. albicans* cells are not currently available in the literature. The behaviour of *C. albicans* has been shown to be similar to that of *S. cerevisiae*,[56,57] a well-studied strain in the context of DEP.[58–60] Based on Fig. 4A, we proceeded to perform experiments to determine the efficiency of washing for different header speeds. We polarized the field at 20 Vpp and 100 kHz and characterized the effect of number of washing cycles on the cell transfer throughput. Since the gradient value of $\sim 5 \times 10^{14}$ V^2 m^{-3} characterized the chip used here when polarized at 20 Vpp, we expected the transfer throughput of cells to significantly diminish above header speeds of 0.05 m s^{-1} since such fluid velocity values would be above the permissible values determined by eqn (4). The maximum shear stress for the velocities used here lies between 1 and 5 dynes per cm^2 which is smaller than the amount of shear stress that can deform the cell. The experimental results are shown in Fig. 4B. As expected, the transfer throughput was inversely proportional to the wash velocity and the number of wash cycles. An increase in both the wash velocity and the number of cycles increased the reproducibility of the operation, as judged from the reduction in the magnitude of the error bars. However, there were still cells transferred at speeds of 0.083 m s^{-1}. This was not expected since the flow velocity significantly overcomes the DEP force expected in the array. Although adhesion forces of cells to carbon could be the ones responsible for this, we speculated that perhaps the flow was not completely entering the electrode array. The computational model described in section 3.5 was then used to visualize the flow of the liquid around the electrodes in the array at the chosen header speed of 0.05 m s^{-1}. Results are shown in Fig. 4C. As the chip and the header moved through the wash plate, the simulated gap between the electrodes was observed exhibiting resistance to the flow that diverted the flow of liquid around rather than in between the electrodes. Thus, the velocity of the liquid in the region between the electrodes remained low even at high header speeds. Due to this phenomenon, the expected effect from increasing the header speed was not observed in the experiment. To summarize, we could optimize the wash step to decrease the contamination; however the contamination could not be completely averted due to the resistance provided to the flow by the dense electrode array. Ongoing work is addressing such problem as detailed in the Discussion section of this work.

4.3 The use of negativeDEP aids the release of cells in the transfer stage

After studying the picking and washing steps of the process, we focused on characterizing the transfer step, where the electrode array containing the *Candida* cells was immersed into the liquid on the transfer plate. Initially, the electric field was turned off and we expected the cells to diffuse away from the electrode. While this led to acceptable results (Fig. 4D), we noticed that some cells remained adhered to the carbon electrodes. This was unacceptable because it could lead to low transfer throughput and fouling of the electrode array for subsequent cycles. By taking advantage of negativeDEP, the forces causing the cells to move away from the field gradient around the electrodes, we were able to improve the transfer

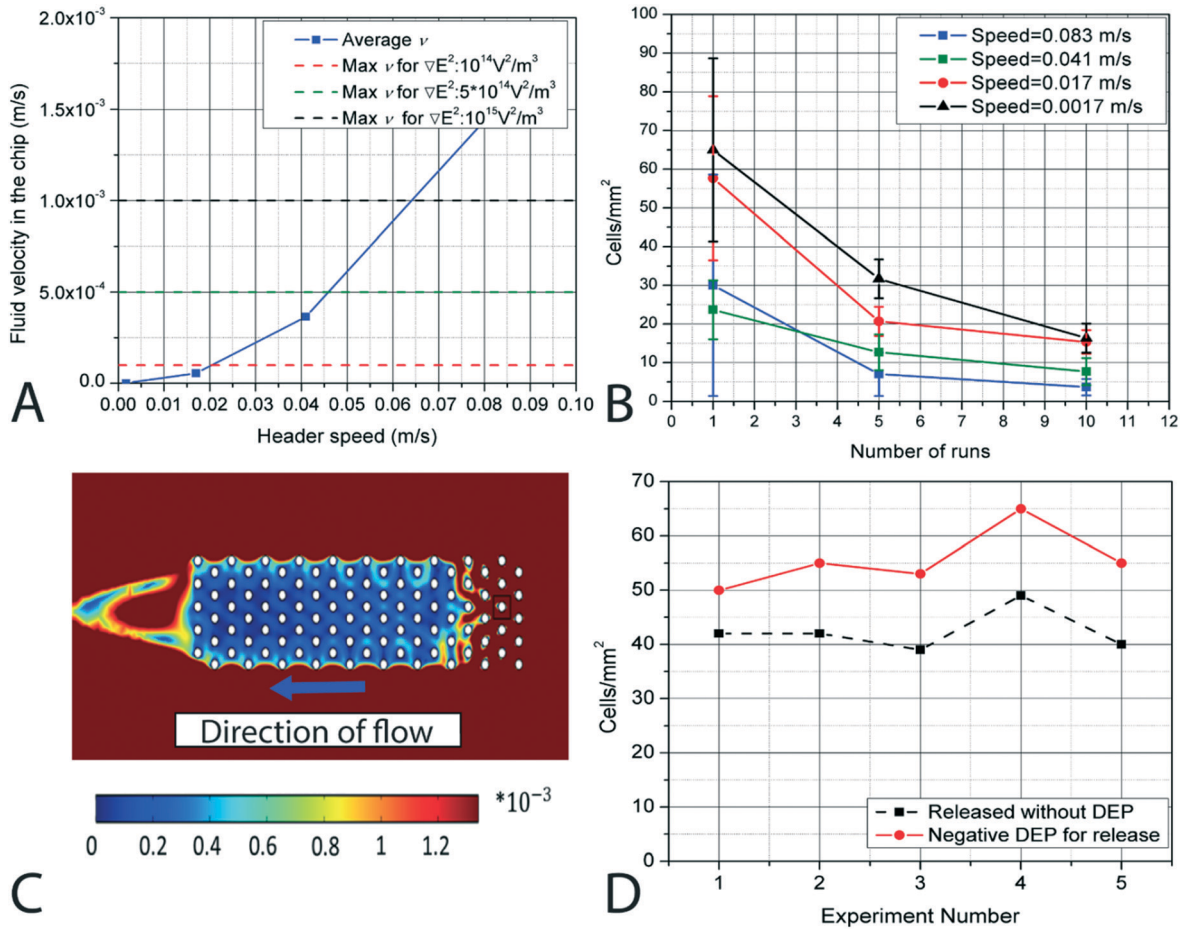

Fig. 4 (A) The plots of the average fluid velocity in the chip for different header speeds. Average velocity in between the electrodes was computed for different header speeds. The horizontal lines in the graph indicate the permissible velocity for the *Candida* cells such that the DEP force remains greater than the drag force in the domain; calculated using eqn (4). (B) The results of a number of runs and different header speeds performed to eliminate contamination during the wash step. The *Y* axis shows the number of cells carried by the chip due to non-specific adhesion for these wash speeds and number of runs. The increase in both speed and number of wash runs reduced the numbers of cells transferred non-specifically, with a speed of 0.083 m s^{-1} and 10 runs providing the best results. (C) The COMSOL simulation comparing the flow within and around the chip, where the chip exhibits resistance and greatly reduces the flow. (D) A comparison of the number of cells transferred with negative DEP and without DEP.

throughput by 25% as illustrated in Fig. 4D when using *C. albicans*. This was possible by switching the frequency of the signal polarizing the electrodes from 100 to 10 kHz. The use of negativeDEP to aid cell release was preferred to the addition of surfactants or reagents like trypsin to the sample since these could increase its electrical conductivity and reduce the strength of the positiveDEP force used to hold the cells in place during transfer. Previous authors who have worked with micromanipulators observed similar issues with cell adhesion during release and used more complicated approaches such as an electrostatic micro actuated plunger,[6] vacuum tools[61] or thermal microgrippers[62] to facilitate cell release.

4.4 Cell separation and single cell transfer are possible operations

Two mixtures were used to demonstrate cell sorting using roboticDEP. *C. tropicalis* cells were separated from 10 μm polystyrene beads by taking advantage of the fact that at 100 kHz *C. tropicalis* exhibited a positiveDEP while the 10 μm polystyrene beads exhibited a negativeDEP. Hence, *C. tropicalis* were picked by the electrode array, washed at 0.05 m s^{-1} and 5 washing cycles, and selectively transferred to the transfer plate, using negativeDEP at f = 10 kHz to aid release. Results are shown in Fig. 5. While the initial ratio of cell to particle concentration in the sample was 15/85, this ratio was flipped to 78/22 after processing with roboticDEP. Such a change clearly indicated the efficacy of this system in selectively picking and transferring targeted cells and separating them from latex particles. A viability assay was then implemented by separating viable RASCs from non-viable ones. At 100 kHz, viable cells and non-viable cells exhibited positive and negative DEP, respectively. This difference in the properties was used to selectively pick and transfer the viable cells. In this case, the wash was done at 20 mm min^{-1} and 2 runs. This speed was obtained through experimental trials,

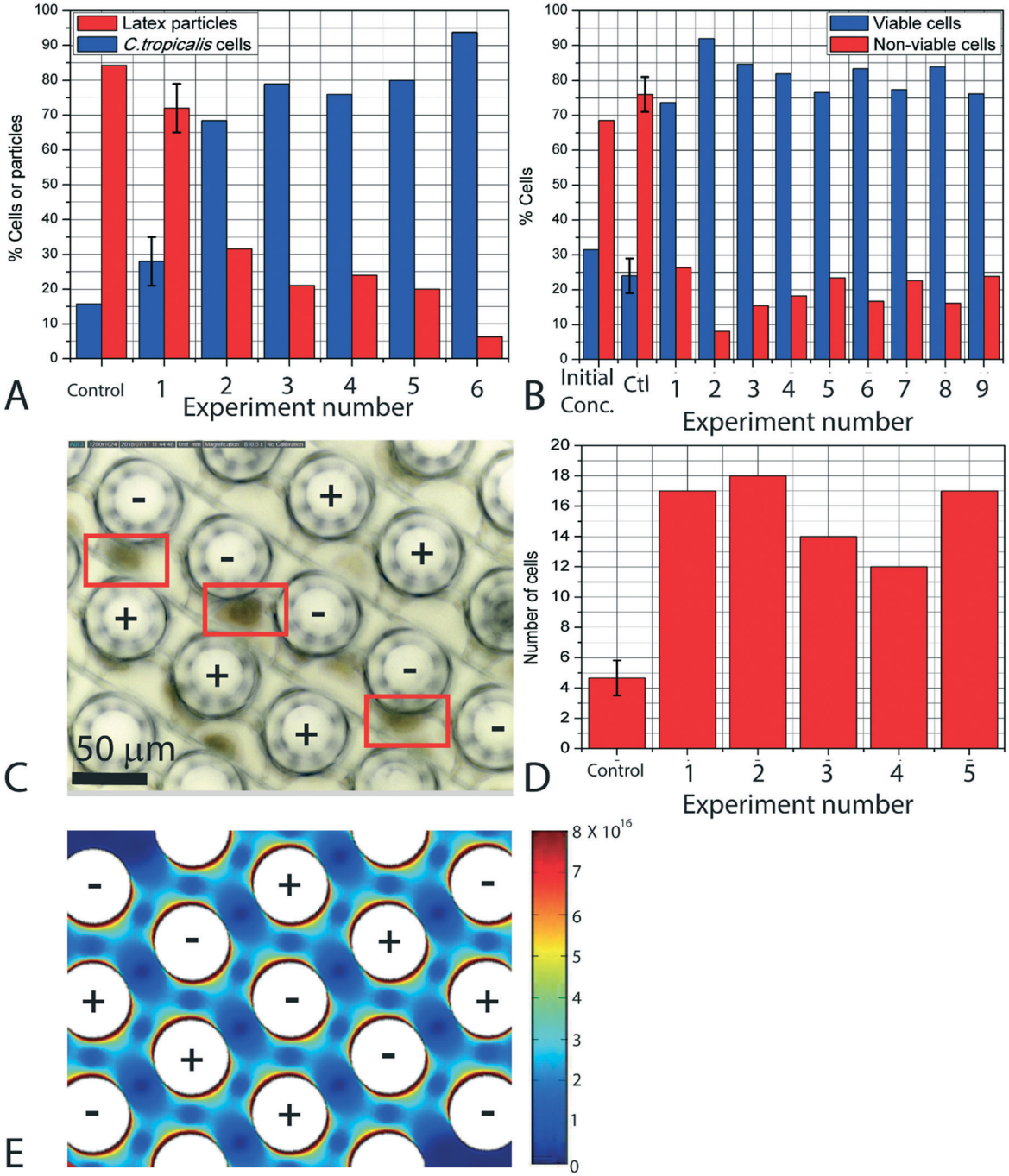

Fig. 5 (A) Results showing separation of *C. tropicalis* from latex particles. The initial distribution of the sample at the pick stage was 15% *Candida* and 85% latex. This drastically changed to an average of 81% (orange slashed line) *Candida* in all 5 independent experiments. (B) Results from the separation of viable RASCs from non-viable ones. Here, the percentage of viable cells was increased from around 30% in the initial sample to an average of 81% from 9 independent experiments. Control experiments were those when the electrode array was not polarized. Reported values for control experiments are the average and error for n = 3 experiments conducted when DEP was off. (C) Rectangles indicate single RASC cells captured at the edge of the electrode. Polarization of the electrodes was as shown. (D) Number of single cells transferred by pick and transfer in 5 independent experiments. Control experiment indicates the number of cells transferred when electrodes were not electrically polarized, n = 3. (E) Electric field gradient as modeled using COMSOL; the highest electric field gradient was around the electrodes and corresponds to the regions where cells were trapped (see (C)). Units are in $V^2\ m^{-3}$.

as the DEP parameters for these cells are not available in the literature. The wash speed and number of cycles used were different from those used when using *Candida* because these cells possess different cell size and cell membrane properties. The change in cell size and cell membrane potential affects the maximum velocity in eqn (4) based on drag and DEP force acting on the cell. Moreover, the RASCs had a diameter comparable to the gap between electrodes and hence we

further suspect the cell size to affect the electric field around it and thus additional components to the DEP force acting on the cell. Results are shown in Fig. 5B and again demonstrate the efficacy of roboticDEP to pick and transfer targeted cells. While the ratio between percentages of viable/nonviable RASCs in the original sample was 30/70, this was flipped to an average of 81/19 after processing. Although both viable and non-viable stem cells were of similar size, the separation of viable RASCs is possible with roboticDEP. Lastly, we demonstrated single cell transfer using roboticDEP. Single viable RASCs were picked from a diluted suspension, shown inside the rectangles in Fig. 5C, and transferred to the transfer plate. A wash of 20 mm min^{-1} was implemented and the electric field was switched off during release, *i.e.* no negative DEP was used during release. Results are shown in Fig. 5D. Starting from a suspension with a concentration of ~103 cells per ml, roboticDEP enabled the selection and transfer of 12–18 cells in each of 5 independent experiments.

5. Discussion

The authors demonstrated the effective use of 3D carbon electrodes on a robotic platform for the selection of targeted cells from a sample and their placement on specific locations. The use of DEP ensured cell selectivity and the robotic arm ensured that the device completed an automated cycle. The sample volume used in this work was 10 μl for practical purposes; the sample volume is expected to depend on the combination of the size of the electrode array, the resolution of the robotic manipulator, and the surface area-to-volume ratio of the sample. Future work will be on studying the rupture of the air–sample interface by different electrode arrays as the surface area/volume ratio changes. This proof of concept for roboticDEP was successfully used in the separation of targeted cell populations from a background at sample concentrations of 10^5 cells per ml, significantly flipping the ratio of the percentage of targeted to non-targeted cells from an initial value of either 15/85 or 30/70 to a final value of ~80/20. One cycle, *i.e.* pick, wash and transfer, of this initial demonstration lasted around 4 minutes and further optimization is expected to drastically reduce this time. The average number of cells transferred was 60 cells per mm^2, which is expected to be increased by augmenting the number of electrodes, establishing better contact between electrode array and cell suspension, and optimizing the trajectory of the robotic manipulator. In terms of single cell processing, we demonstrated the pick and transfer of up to 18 single RASC cells per experiment when using a cell concentration of 10^3 cells per ml in the original sample. These promising results encourage further research and development in this topic since a roboticDEP setup can yield benefits in the integration of DEP selectivity in current laboratory infrastructure. For example, an automated DEP-based sorter like the one described here can pick selected cells from a mixture and directly transfer them to sites for bioanalysis or further processing. For multiple types of cells with different DEP behaviours, the sorter can pick and drop each type at different desired location automatically. Furthermore, with modification of the electrodes to capture single cells, several single cells can be sorted and transferred in parallel. With sufficient control on the transfer location of the cell, cells or particles could be transferred to form micro patterns.

The viability of the cells during operation is an important factor to consider in the pick and transfer experiments. Since the setup represents a vented system, the cell culture is exposed to the environment during operation, which could lead to cell contamination or evaporation of the cell culture. In our current setup, we did not notice significant cell contamination or evaporation of cell culture. This was likely due to the short transfer times used. However, this issue would be an important consideration for future development of this technique. Having an enclosed system to reduce the possibility of contamination and/or implementing the complete pick and transfer in a liquid medium are possibilities to address. Additionally, the sample and transfer plates need to be clean to avoid cell contamination. Contaminants can affect the way the cell culture interacts with the surface of the plates and clean surfaces ensure proper control of the surface area/volume ratio of the sample when placed on these plates. One-time disposable consumables are recommended. The exposure of cells to an electric field is also an important parameter that affects cell viability. As stated previously, a general rule of thumb is for the electric field not to exceed a threshold value of around 100 kV m^{-1} to maintain the integrity of the cell membrane[32] but such a threshold can vary with the type of cell and experimental conditions. As an example, Lu *et al.* reported that cell exposure at 8 V peak to peak at frequencies of 50–100 kHz (with electric field ~10^5 V m^{-1}) for a time >5 min can affect the cell viability.[19] Nerguizian *et al.*[63] studied the effect of an electric field on the regulation in gene expression of different cell strains and found that an exposure of around 60 minutes at 10 volts peak with a medium electrical conductivity of 10 mS m^{-1} can affect the gene expression of the cell. In the experiments reported here, cells were exposed to an electric field lower than 100 kV m^{-1} for the entire experiment time (<4 min). Nevertheless, the effect of electric field exposure on the cell viability, proliferation and gene expression needs to be studied further in future studies.

While DEP has been shown to provide highly specific separations by multiple authors, it does require control of the ratio between the electrical polarizability of the cell and the suspending medium. Active trapping cells of cells on the electrodes using positiveDEP requires a higher polarizability from the cell. This presents a challenge when working with a biological medium, usually of high electrical conductivity, since positiveDEP will be negligible. Hence, the technology platform presented here is currently limited to protocols that include sample preparation in the form of cell resuspension in DEP buffers with low electrical conductivity and optimized pH and osmolality values, like the sugar solution used here and demonstrated by multiple authors before.[19,64,65] Of note,

sample preparation steps are also required by flow cytometry, *i.e.* incubation with labels, and traditional DEP technologies, but important advantages of roboticDEP are label-free sorting and spatiotemporal control of single cells at all times.

Ongoing work is on increasing system efficiency by refining the different steps in roboticDEP. The current device has a resolution of 100 μm in its three-dimensional movement due to the limitation of the robotic setup. Since the electrode footprint is around 50 μm (diameter) and 100 μm (height), even the smallest error in the movement of the robotic arm can lead to significant error in resolution. By improving the resolution of the robotic setup, the movement of the header can be refined. For example, liquid handling robots feature movement resolutions up to 1 μm,[66] whereas high precision robots for handling micro objects have been developed with movement resolution up to 10 nm.[67] The geometry of 3D carbon electrodes can also be designed depending on the application and size of targeted cells; electrode arrays featuring post electrode diameters down to 1 μm are reported[68] as well as the possibility to fabricate diverse cross sections[69] and even cones.[70] This opens a myriad of possibilities by allowing the translational motion, using a robot, of different designs of electric field gradients, determined by the properties of the electrode array. Nevertheless, the dimensions and geometry of both the electrode array and the individual electrodes must be optimized depending on the targeted cells and the properties of the other cells in the suspension. For example, the field gradient generated at the edges of the cylindrical electrodes used here was high enough to trap single stem cells. The volume of the DEP trap around the electrode approximated the volume of a single RASC (~34 000 μm^3 based on a sphere with a diameter of around 20 μm). However, as the cell volume of the targeted cells decreases, as in the case of *Candida* with a volume of only ~300 μm^3, the number of cells captured at the electrodes can be quite large (Fig. 3D *vs.* Fig. 5C). The use of the computational model described above will not only facilitate the modelling of the field gradient when using different polarization schemes of a given electrode array but also optimize future device designs. The geometry of the electrodes can thus be tailored depending on the kind of cell targeted and whether transfer of a single cell or a population of cells is desired. Of note, we previously reported how a conical electrode geometry with an optimized tip angle can yield local field gradients that result in the DEP trapping of small cells such as yeast.[31]

The computational model will also enable the design of the shape of array to obtain more reproducible washes by enabling liquid to permeate through the array. By increasing the gap between the electrodes, the resistance to the flow of medium will decrease, enabling better washes during the wash step. Using slender structures with a high aspect ratio[71] as electrodes can also enable capture of single cells and enable better washes. Additionally, using streamlined lens or arrow-shaped structures for the electrodes can also enable better flow of the medium through the electrode domain. These changes will also affect the electric field and field gradient in the domain. The throughput of a pick and transfer platform is expected to significantly increase when compared to traditional systems since the number of electrodes in the array can be significantly scaled up (no physical limits given by the dimensions of the channel) and the array itself can be made to sweep a large volume of liquid while trapping specific cells (instead of forcing the sample through a channel).

RoboticDEP is a vented system that minimizes issues with bubbles common in microfluidics-based systems. However, this approach introduces concerns about the effect that breaking a liquid–air interface can have on system efficiency. This is because pressure pulses during piercing the interface can release cells that were previously trapped. Such behaviour is observed during the pick and transfer step. The cells experience the effect of piercing as they spill when the electrodes puncture the drop of suspension at the pick section and when the electrodes with attached cells enter the medium at the transfer plate. Reducing the approach speed of the header to alleviate the piercing proved to be beneficial to a certain extent. Operating the pick, wash and transfer steps entirely in the liquid domain would be an ideal solution for this issue. However, care must be taken in such an approach to avoid the mixing of liquids between different steps. It is envisioned that this can be achieved by having the transfer station at a higher level than the pick station. Another approach to reduce the effect of piercing in the case of the pick step is to use a small cell reservoir in place of a drop of culture. Lastly, improving the separation efficiency will also require minimizing the non-specific cell adhesion. It is thus important to treat all surfaces in direct contact with the liquid, similar to the treatment done by Kim *et al.*[72] for microgrippers, to prevent non-specific adhesion. Given that cell adhesion is the primary mechanism behind cell placement, electrode surfaces must be treated to enhance the electrode performance. Another approach to release the non-specific cells is the use of mechanical vibrations.[73] However, care should be taken to retain the cells trapped by DEP while the contaminants release owing to inertia.

6. Concluding remarks

Here the concept of automated pick and transfer of targeted cells is demonstrated with roboticDEP. The authors successfully selected and transferred targeted cells from a suspension. The cells studied here were two different *Candida* strains, *C. albicans* and *C. tropicalis*, and rat adipose stem cells (RASCs). Besides providing adequate properties to demonstrate the concept of roboticDEP, *Candida* strains were studied due to their relevance in candidiasis, a common infection of the skin, oral cavity and esophagus, gastrointestinal tract, vagina and vascular system of humans.[74] Mammalian adipose tissue-derived stem cells such as RASCs are multipotent cells with the potential to differentiate into diverse cell lineages such as endothelial cells, cardiomyocytes, adipocytes and osteoblasts. Their abundance and ease of sampling provide a scope for regenerative medicine and

tissue engineering, which makes the study of these cells important.[75,76]

The concept of roboticDEP can enable the programming of cell transfer among different vials, and the sharing of a common platform with liquid handling robots encourages the integration of these systems to engineer a precise sample in terms of medium volume and number and type of cells. The use of roboticDEP in sample preparation can also facilitate the process to connect the cell genotype and its DEP signature given by its phenotype. Ongoing work is on the demonstration of electrical lysis in roboticDEP. This builds up on the electrical lysis of cells using carbon electrodes such as those used by Mernier *et al.*[48] The envisioned function is to pick targeted cells and once transferred to a specific location, lyse them to release their intracellular components.

Conflicts of interest

There are no conflicts to declare.

Acknowledgements

The authors would like to acknowledge the help received from colleagues at Clemson University: Mrs. Cassie Gregory at the Cell and Tissue Culture Laboratory in the Department of Bioengineering for culturing rat adipose stem cells and the Blenner Lab group in the Department of Chemical Engineering for facilitating the culture of *Candida* cells.

References

1 B. Solano and D. Wood, *Microelectron. Eng.*, 2007, **84**, 1219–1222.
2 D. Gao, F. Jin, M. Zhou and J. Yuyang, *Analyst*, 2019, **144**, 766–781.
3 S. Grover, A. Skirtach, R. Gauthier and C. Grover, *J. Biomed. Opt.*, 2001, **6**, 14–22.
4 S. C. Chapin, V. Germain and E. R. Dufresne, *Opt. Express*, 2006, **14**, 13095–13100.
5 E. W. H. Jager, O. Inganäs and I. Lundström, *Science*, 2000, **288**, 2335–2338.
6 Y. Zhang, B. K. Chen, X. Liu and Y. Sun, *IEEE Trans. Robot.*, 2010, **26**, 200–207.
7 E. B. Steager, M. S. Sakar, C. Magee, M. Kennedy, A. Cowley and V. Kumar, *Int. J. Rob. Res.*, 2013, **32**, 346–359.
8 K. Mølhave, T. Wich, A. Kortschack and P. Bøggild, *Nanotechnology*, 2006, **17**, 2434.
9 K. S. Colinjivadi, L. Jeong-Bong and D. Rockford, *Microsyst. Technol.*, 2008, **14**, 1627–1633.
10 Z. R. Gagnon, *Electrophoresis*, 2011, **32**, 2466–2487.
11 R. Pethig, *Biomicrofluidics*, 2010, **4**, 22811.
12 M. Elitas, R. Martinez-Duarte, N. Dhar, J. D. McKinney and P. Renaud, *Lab Chip*, 2014, **14**, 1850–1857.
13 R. Martinez-Duarte, P. Renaud and M. J. Madou, *Electrophoresis*, 2011, **32**, 2385–2392.
14 H. Li and R. Bashir, *Sens. Actuators, B*, 2002, **86**, 215–221.
15 Y. Yildizhan, N. Erdem, M. Islam, R. Martinez-Duarte and M. Elitas, *Sensors*, 2017, **17**, 1–13.
16 J. Suehiro, R. Hamada, D. Noutomi, M. Shutou and M. Hara, *J. Electrost.*, 2003, **57**, 157–168.
17 R. C. Gallo-Villanueva, N. M. Jesus-Perez, J. I. Martinez-Lopez, A. Pacheco and B. H. Lapizco-Encinas, *Microfluid. Nanofluid.*, 2011, **10**, 1305–1315.
18 L. A. Flanagan, J. Lu, L. Wang, S. A. Marchenko, N. L. Jeon, A. P. Lee and E. S. Monuki, *Stem Cells*, 2008, **26**, 656–665.
19 J. Lu, C. A. Barrios, A. R. Dickson, J. L. Nourse, A. P. Lee and L. A. Flanagan, *Integr. Biol.*, 2012, **4**, 1223.
20 R. S. W. Thomas, P. D. Mitchell, R. O. C. Oreffo and H. Morgan, *Biomicrofluidics*, 2010, **4**, 22806.
21 S. K. Srivastava, P. R. Daggolu, S. C. Burgess and A. R. Minerick, *Electrophoresis*, 2008, **3**, 401–404.
22 R. Pethig, V. Bressler, C. Carswell-Crumpton, Y. Chen, L. Foster-Haje, M. E. García-Ojeda, R. S. Lee, G. M. Lock, M. S. Talary and K. M. Tate, *Electrophoresis*, 2002, **23**, 2057–2063.
23 F. H. Labeed, J. Lu, H. J. Mulhall, S. A. Marchenko, K. F. Hoettges, L. C. Estrada, A. P. Lee, M. P. Hughes and L. A. Flanagan, *PLoS One*, 2011, **6**, 1–11.
24 P. R. C. Gascoyne, J. Noshari, T. J. Anderson and F. F. Becker, *Electrophoresis*, 2009, **30**, 1388–1398.
25 R. Martinez-Duarte, *Electrophoresis*, 2012, **33**, 3110–3132.
26 N. Manaresi, A. Romani, G. Medoro, L. Altomare, A. Leonardi, M. Tartagni and R. Guerrieri, *IEEE. J. Solid-State Circuits*, 2003, **38**, 2297–2305.
27 T. P. Hunt and R. M. Westervelt, *Biomed. Microdevices*, 2006, **8**, 227–230.
28 T. Schnelle, T. Muller, H. Rolf, V. Andreas and G. Fuhr, *Biochim. Biophys. Acta, Gen. Subj.*, 1999, **1428**, 99–105.
29 A. Menachery, D. Graham, S. Messerili, R. Pethig and P. J. Smith, *IET Nanobiotechnol.*, 2011, **5**, 1–7.
30 A. Castellanos, A. Ramos, A. Gonz and N. G. Green, *J. Phys. D: Appl. Phys.*, 2003, **36**, 2584–2597.
31 R. Natu, M. Islam and R. Martinez-Duarte, in *ASME 2015 International Mechanical Engineering Congress and Exposition*, Houston, USA, 2015.
32 B. Valic, M. Golzio, M. Pavlin, A. Schatz, C. Faurie, B. Gabriel, J. Teissie, R. Marie-Pierre and M. Damijan, *Eur. Biophys. J.*, 2003, **32**, 519–528.
33 D. W. Lee and Y. H. Cho, *Sens. Actuators, B*, 2007, **124**, 84–89.
34 L. Adamo, O. Naveiras, P. L. Wenzel, S. McKinney-Freeman, P. J. Mack, J. Gracia-Sancho, A. Suchy-Dicey, M. Yoshimoto, M. W. Lensch, M. C. Yoder, G. García-Cardeña and G. Q. Daley, *Nature*, 2009, **459**, 1131–1135.
35 S. Fukuda and G. W. Schmid-Schönbein, *Proc. Natl. Acad. Sci. U. S. A.*, 2003, **100**, 13152–13157.
36 R. E. Gerszten, Y. C. Lim, H. T. Ding, K. Snapp, G. Kansas, D. A. Dichek, C. Cabañas, F. Sánchez-Madrid, M. A. Gimbrone, A. Rosenzweig and F. W. Luscinskas, *Circ. Res.*, 1998, **82**, 871–878.
37 R. P. Wolfe and T. Ahsan, *Biotechnol. Bioeng.*, 2013, **110**, 1231–1242.

38 R. Natu, M. Islam and R. Martinez-Duarte, *Anal. Chem.*, 2019, **91**, 4357–4367.
39 M. Islam, R. Natu and R. Martinez-Duarte, in *Carbon : The next Silicon? Book-2 Applications*, 2015, vol. C, pp. 79–100.
40 J. Gilmore, M. Islam, J. Duncan, R. Natu and R. Martinez-Duarte, *Electrophoresis*, 2017, **38**, 1–4.
41 R. Martinez-Duarte, J. Andrade-Roman, S. O. Martinez and M. Madou, in *NSTI-Nanotech*, Boston, USA, 2008.
42 R. Martinez-Duarte, R. A. Gorkin, K. Abi-Samra and M. J. Madou, *Lab Chip*, 2010, **10**, 1030–1043.
43 R. Martinez-Duarte, R. A. Gorkin, K. Abi-Samra and M. J. Madou, in *Transducers 2009*, Denver, USA, 2009.
44 M. Islam, R. Natu, L.-M. M. Fernanda and M.-D. Rodrigo, *Biomicrofluidics*, 2016, **10**, 33107.
45 R. Martinez-Duarte, *ECS Trans.*, 2014, **61**, 11–22.
46 M. D. C. Jaramillo, E. Torrents, R. Martinez-Duarte, M. J. Madou and A. Juarez, *Electrophoresis*, 2010, **31**, 2921–2928.
47 R. Martinez-Duarte, F. Camacho-Alanis, P. Renaud and A. Ros, *Electrophoresis*, 2013, **34**, 1113–1122.
48 G. Mernier, R. Martinez-Duarte, R. Lehal, F. Radtke and P. Renaud, *Micromachines*, 2012, **3**, 574–581.
49 S. Silva, M. Negri, M. Henriques, R. Oliveira, D. W. Williams and J. Azeredo, *FEMS Microbiol. Rev.*, 2012, **36**, 288–305.
50 M. Islam, J. Gilmore, K. Wallace and R. Martinez-Duarte, in *MicroTas*, Savannah, USA, 2017.
51 M. P. Hughes and H. Morgan, *Anal. Chem.*, 1999, **71**, 3441–3445.
52 I. Ermolina and H. Morgan, *J. Colloid Interface Sci.*, 2005, **285**, 419–428.
53 L. Cui, D. Holmes and H. Morgan, *Electrophoresis*, 2001, **22**, 1135–1146.
54 R. Natu and R. Martinez-Duarte, *Micromachines*, 2016, 217.
55 R. Martinez-Duarte, *PhD, Mechanical Engineering*, University of California, Irvine, 2010.
56 C.-C. Chung, I.-F. Cheng, C.-C. Lin and H.-C. Chang, *Microfluid. Nanofluid.*, 2011, **10**, 311–319.
57 O. Français and B. Le Pioufle, *Lab Chip*, 2013, **13**, 901–909.
58 G. H. Markx, Y. Huang, X. Zhou and R. Pethig, *Microbiology*, 1994, **140**, 585–591.
59 Y. Huang, J. M. Yang, P. J. Hopkins, S. Kassegne, M. Tirado, A. H. Forster and H. Reese, *Biomed. Microdevices*, 2003, **5**, 217–225.
60 Y. Huang, R. Hölzel, R. Pethig and X. B. Wang, *Phys. Med. Biol.*, 1992, **37**, 1499–1517.
61 W. Zesch, M. Brunner and A. Weber, in *IEEE lntemational Conference on Robotics and Automation*, Albuquerque, New Mexico, 1997, pp. 1761–1766.
62 L. Beatriz and N. Chaillet, *IEEE Trans Robot*, 2008, **24**, 897–902.
63 V. Nerguizian, I. Stiharu, N. Al-azzam, B. Yassine-diab and A. Alazzam, *Analyst*, 2019, DOI: 10.1039/c9an00320g.
64 R. Pethig and M. S. Talary, *IET Nanobiotechnol.*, 2007, **1**, 2–9.
65 L. Wang, L. A. Flanagan, N. L. Jeon, E. Monuki and A. P. Lee, *Lab Chip*, 2007, **7**, 1114–1120.
66 F. Kong, L. Yuan, Y. F. Zheng and W. Chen, *J. Lab. Autom.*, 2012, **17**, 169–185.
67 A. Codourey, W. Zesch, R. Bÿchi and R. Siegwart, in *Seminar on Handling and Assembly of Microparts*, Vienna, Austria, 1994.
68 L. Amato, S. S. Keller, A. Heiskanen, M. Dimaki, J. Emnéus, A. Boisen and M. Tenje, *Microelectron. Eng.*, 2012, **98**, 483–487.
69 R. Natu, M. Islam, J. Gilmore and R. Martinez-duarte, *J. Anal. Appl. Pyrolysis*, 2018, **131**, 17–27.
70 R. Martinez-Duarte, *Micromachines*, 2014, **5**, 766–782.
71 L. Amato, A. Heiskanen, R. Hansen, L. Gammelgaard, T. Rindzevicius, M. Tenje and J. Emne, *Carbon*, 2015, **94**, 792–803.
72 K. Kim, X. Liu, Y. Zhang, Y. Sun and J. Micromechanics, *Microengineering*, 2008, **18**, 55013.
73 D. S. Haliyo, S. Regnier and J.-C. Guinot, *Eur. J. Mech. A, Solids*, 2003, **22**(6), 903–916.
74 R. A. Calderone and W. A. Fonzi, *Trends Microbiol.*, 2001, **9**, 327–335.
75 J. M. Gimble, A. J. Katz and B. A. Bunnell, *Circ. Res.*, 2007, **100**, 1249–1260.
76 M. E. Danoviz, J. S. Nakamuta, F. L. N. Marques, L. Santos, C. Erica, A. A. Santos, E. L. Antonio, I. T. Schettert, P. J. Tucci and E. Jose, *PLoS One*, 2010, **5**, 1–9.